25th ABCM International Congress of Mechanical Engineering
October 20-25, 2019, Uberlândia, MG, Brazil

COB-2019-0809
CONTINUOUS AND DISCRETE SOLUTION FOR A PLANE JET

Gabriel Marcos Magalhães
Jessica Guarato de Freitas Santos
Aristeu da Silveira Neto
Faculty of Mechanical Engeneering. Federal University of Uberlândia (UFU), Av. João Naves de Ávila 2121, 38400-902, Uberlândia-MG, Brazil
gabrielm@ufu.br, jessica.guarato@ufu.br, aristeus@ufu.br

Abstract. *In the present work, continuous solutions were developed for a plane jet in laminar and turbulent regimes using the self-similarity solution technique. The results obtained through the proposed solutions differ from the results presented in the literature. Furthermore, two different models of the Unsteady Reynolds Averaged Navier-Stokes (URANS) class were implemented in an in-house code and applied in a simulation of a turbulent plane jet. Despite the small difference in the transport equations of the standard $k-\epsilon$ model and the realizable $k-\epsilon$ model, it is known that each model behaves differently depending on the type of problem. Therefore, the objective of the present work is to compare the results of a numerical solution of a turbulent plane jet, using the aforementioned variations of the $k-\epsilon$ model, with the continuous solution. The normalized mean velocity profile along the jet centerline was obtained for all the three cases and compared with experimental data found in the literature. In addition to the experimental data, the numerical results, which are discrete results, were also compared with the continuous solution obtained by the authors of the present work using the similarity solution technique.*

Keywords: *URANS, plane jet, similarity solution, k-epsilon models, turbulence*

1. INTRODUCTION

The plane jet belongs to a class of free shear flows, in other words, flows in the absence of walls and pressure gradients. The simulation of two-dimensional jets can provide a good initial prediction for several industrial problems. However, the simulations of this type of problem become complex when they involve turbulence, causing the computational cost and the demanded time considerably high. Therefore, an alternative to model the turbulence with a reasonable computational cost is to use RANS (Reynolds Averaged Navier-Stokes) class models, which provide the average behavior of the flow and can be easily applied in two-dimensional simulations.

As presented by American Society of Heating and Engineers (1989), free jets can be divided into four different zones: the first zone corresponds to a short region in which the mean velocity remains approximately constant, the second zone is a transitional zone, the third zone is related to a fully developed turbulent flow, and the last zone is the terminal zone. The third one is also considered the self-similar zone, and because of that is the main jet region in engineering applications. Liu *et al.* (1996) compared the performance of the standard $k-\epsilon$ model with the Lam and Bremhorst (1981) low Reynolds number model considering and desregarding wall functions in predicting a plane-free jet and a plane-wall jet behavior, in the self-similar zone. Velocity decay, velocity profile and spread rate were evaluated and compared to available experimental data. The simulations predicted the velocity decay and the velocity profile well, but overpredicted the jet spread. Wilcox Wilcox (1994) compared the spreading rate for plane jets and round jets using the Standard $k-\epsilon$ model. The results presented good agreement with experimental data. The spreading rate obtained from numerical simulations of the round jet was 25 % to 40 % higher than the spreading rate measured by experiments. Block (2006) analyzed the performance of the Prandtl mixing length model, the standard $k-\epsilon$ model and the Renormalization Group (RNG) $k-\epsilon$ model for the solution of a round jet. Basically, it was concluded that the Standard $k-\epsilon$ model presented better agreement with experimental data. Ströher *et al.* (2009) evaluated numerically a incompressible axysimmetric turbulent free jet using three RANS based turbulence models: standard $k-\epsilon$, realizable $k-\epsilon$ and $v2-f$. The numerical results were compared with available experimental data for two jets issuing from a nozzle with fully-developed and "top-hat" velocity profile. Only the results obtained using the two $k-\epsilon$ models presented good agreement with the experimental ones considering "top-hat" jet origin boundary condition.

The purpose of the present work is to compare the results of some plane jet characteristics provided by numerical simulations using two $k-\epsilon$ turbulence models: standard $k-\epsilon$ and realizable $k-\epsilon$. The simulations were performed in an in-house computational code (MFSim) developed using the finite volume method to discretize the equations, staggered

grid and parallel processing. In addition, a continuous solution is proposed for turbulent plane jets using the self-similarity solution method. Unlike the continuous solutions already presented in the literature, in the present work, the integral of momentum flux was not considered unitary. A comparison of the continuous solution against the experimental data presented in the literature with the results of the numerical simulations using the two models allows to verify which one presents better agreement of the results in two aspects. These aspects are the mean velocity profile evaluated in different sections of the computational domain, and the velocity decay at the jet center line.

2. MATHEMATICAL MODEL

This section presents the mathematical models applied to the case study. Considering one phase and an isothermal flow, the fluid solution can be expressed by the continuity and Navier-Stokes equations. The Navier-Stokes equations are sufficient to solve turbulent flows using Direct Numerical Simulations (DNS). This simulation technique has a high computational cost, because it needs to resolve all the turbulence eddies and this requires a very fine grid. An alternative method is the decomposition of the power spectra of the eddy-velocity into two bands, which is related to obtaining the filtered equations and the concept of filtering. This leads to the so-called turbulence closure problem. An alternative to treat the turbulence closure problem is using the Boussinesq hypothesis to model the global Reynolds stress shown in Eq. (1)).

$$\tau_{ij} = \mu_t \left(\frac{\partial \bar{u}_i}{\partial x_j} + \frac{\partial \bar{u}_j}{\partial x_i} \right) - \frac{2}{3} k \delta_{ij}, \tag{1}$$

where μ_t is the turbulent dynamic viscosity, δ_{ij} is the Kronecker delta and k is the turbulent kinetic energy.

The turbulent dynamic viscosity is a property of the flow and is calculated by the closure models. In the present work, two $k - \epsilon$ models are used. The $k - \epsilon$ model and its variants are two transport equations models and they belong to both Reynols Average Navier Stokes (RANS) and Unsteady RANS (URANS) class method. The first equation transports k and the second transports its dissipation rate, ϵ. The k and ϵ values are used to obtain the turbulent dynamic viscosity.

For a Newtonian fluid and an incompressible flow, the filtered continuity and Navier-Stokes equations with the Boussinesq hypothesis are given by

$$\frac{\partial (\rho \bar{u}_i)}{\partial x_i} = 0, \tag{2}$$

$$\frac{\partial (\rho \bar{u}_i)}{\partial t} + \frac{\partial (\rho \bar{u}_i \bar{u}_j)}{\partial x_j} = -\frac{\partial \bar{p^*}}{\partial x_i} + \frac{\partial}{\partial x_j} \left[(\mu + \mu_t) \left(\frac{\partial \bar{u}_i}{\partial x_j} + \frac{\partial \bar{u}_j}{\partial x_i} \right) \right], \tag{3}$$

where the bar is the filter, ρ is the fluid density, u_i corresponds to the i component of the velocity vector, p^* is the modified pressure and μ is the fluid dynamic viscosity. When the Eqs. (2) and (3) are solved with URANS method, filter corresponds to the average.

2.1 Exact Solution

Considering the differential mathematical model for an incompressible plane jet, in a turbulent regime, presented by Eqs. (2) and (3), it is possible to simplify these equations with hypothesis and assumptions.

It is considered that the process of diffusive transport promoted by turbulence is orders of magnitude larger than the pure molecular diffusive process. Thus, the term involving molecular diffusion will not be considered. The advective term is simplified in accordance with the physics of this problem. In other words, the flow occurs in the $x - y$ plane and the average behavior is considered to be in steady-state. Therefore, the mass balance equation and the filtered Navier-Stokes equation for x-direction results in

$$\frac{\partial \bar{u}}{\partial x} + \frac{\partial \bar{v}}{\partial y} = 0, \tag{4}$$

$$\bar{u} \frac{\partial \bar{u}}{\partial x} + \bar{v} \frac{\partial \bar{u}}{\partial y} = \frac{\partial}{\partial y} \left[\nu_T \left(\frac{\partial \bar{u}}{\partial y} \right) \right]. \tag{5}$$

For the continuous solution, a closure model with zero transport equation is used. The turbulent kinematic viscosity (ν_T) is modeled according to Prandtl-Reichardt model and is given by:

$$\nu_T = \chi \, \delta(x) \, (U_{max} - U_{min}), \tag{6}$$

where χ is a constant of the model which depends on the flow, $\delta(x)$ is the distance between the center line of the jet and the point wich $u(x,y) = 0.01\,U_{min}$, U_{max} is the maximum speed and U_{min} is the minimum speed in the averaged flow.

The plane jets are free shear flows and its mean velocity profile, considering a turbulent regime, is self similar from $x/d = 5$. This characteristic allows the solution technique by self-similarity to be used. This technique proposes a self-similarity variable η and a self-similarity function $F(\eta)$. In the present work, the following definitions were adopted:

$$\eta = \frac{y}{\delta(x)} \qquad \text{and} \qquad F'(\eta) = \frac{\bar{u}(x,y)}{U_c(x)},$$

where $U_c(x)$ is the velocity at jet center line.

The next step of the self-similarity solution is to make Eqs. (4) and (5) as a function of η and $F'(\eta)$. This process leads to an Ordinary Differential Equation (ODE):

$$F''' + \frac{\delta}{U_c\chi}\frac{dU_c}{dx}(FF'' - F'^2) + \frac{1}{\chi}\frac{d\delta}{dx}FF'' = 0. \tag{7}$$

One requirement of the self-similarity solution is that the coefficients of the ODE, given by Eq. (7), be constants. Assuming κ and β constants, it is considered that

$$\frac{1}{\chi}\frac{d\delta}{dx} = \kappa, \tag{8}$$

$$\frac{\delta}{U_c\chi}\frac{dU_c}{dx} = \beta. \tag{9}$$

Integrating Eq. (8) and using the boundary condition, $\delta(x=0) = 0$, it can be found that

$$\delta(x) = Ax, \tag{10}$$

where A is a experimental constant.

It can be found, from experimental data, that the spreading rate for turbulent plane jets is, approximately, 0.1, as presented by Wilcox (1994). Experimental data enables to determine the constant A of Eq. (10). According to measurements of Bradbury (1965), this constant is $A = 0.109$. Thus,

$$\delta(x) = 0.109x. \tag{11}$$

To proceed with the resolution, it is convenient to adopt a simplified hypothesis: the linear momentum of the jet is constant. This hypothesis is based on the Reynolds Transport Theorem (RTT) applied for linear momentum and this means that

$$J = \rho\int_{-\infty}^{\infty} u^2 d\tilde{A} = \text{constant}. \tag{12}$$

Using mathematical arrangements in Eqs. (8), (9) and (12), the ODE can be rewritten as

$$F''' + \frac{A}{2\chi}FF'' + \frac{A}{2\chi}F'^2 = 0, \tag{13}$$

with initial and boundary conditions, considering the domain centered in $y = 0$, given by

$$\eta = 0 \rightarrow F = 0 \qquad \text{null velocity } \bar{v} \text{ in y = 0}, \tag{14a}$$

$$\eta = \infty \rightarrow F' = 0 \qquad \text{null velocity } \bar{u} \text{ in } y \rightarrow \infty, \tag{14b}$$

$$\eta = -\infty \rightarrow F' = 0 \qquad \text{null velocity } \bar{u} \text{ in } y \rightarrow -\infty, \tag{14c}$$

$$\eta = 0 \rightarrow F'' = 0 \qquad \text{null derivative } \left(\frac{\partial\bar{u}}{\partial y}\right) \text{ in } y = 0, \tag{14d}$$

$$\eta = 0 \rightarrow F' = 1 \qquad \bar{u} = U_c \text{ in } y = 0. \tag{14e}$$

Integrating the Eq. (13) and using the previously exposed conditions, the velocity profile is given by

$$\frac{\bar{u}(x,y)}{U_c(x)} = sech^2\left(0.96073\,\eta\right), \tag{15}$$

where

$$\eta = 9.174\,\frac{y}{x}. \tag{16}$$

Therefore, it is possible to define the continuous solution of the velocity at the jet center line. However, it is convenient to present the velocity profile in a dimensionless form, in order to compare results. In this way, the ratio between U_c and the jet mean velocity at the inlet U_j is given as a function of x and the jet nozzle width d. Andrade (1939) explains that it is not convenient to assume the effective origin of the jet at $x = 0$. He suggests that the continuous solution is closer to experimental data when using a x_o value added to x/d. Besides that, according to Tennekes and Lumley (1972), the self-similarity begins from $x/d = 5$ for turbulent plane jets.

Considering that the velocity at the jet center line begins to decay from $x/d = 5$, it can be written as

$$\frac{U_c(x)}{U_j} = 2.5711 \left(\frac{x}{d} + 1.61054\right)^{-1/2}, \tag{17}$$

where U_j is the mean jet velocity at the nozzle.

The continuous solutions represented by Eqs. (15) and (17) will be posteriorly compared with experimental and computational results.

2.2 Numerical modeling

As previously explained, the values of k and ϵ are used to calculate the turbulent dynamic viscosity (μ_t) of the Eq. (3). In a general form, the two transport equations for $k - \epsilon$ models can be written as

$$\frac{\partial(\rho k)}{\partial t} + \bar{u}_j \frac{\partial(\rho k)}{\partial x_j} = \frac{\partial}{\partial x_j}\left[\left(\mu + \frac{\mu_t}{\sigma_k}\right)\frac{\partial k}{\partial x_j}\right] + P_k + D_k, \tag{18}$$

$$\frac{\partial(\rho \epsilon)}{\partial t} + \bar{u}_j \frac{\partial(\rho \epsilon)}{\partial x_j} = \frac{\partial}{\partial x_j}\left[\left(\mu + \frac{\mu_t}{\sigma_\epsilon}\right)\frac{\partial \epsilon}{\partial x_j}\right] + P_\epsilon + D_\epsilon, \tag{19}$$

where σ is a constant, P is the production term, D is the dissipation term, and their expressions depend on each model. In the present work, source terms were not considered.

The calculation of turbulent dynamic viscosity as function of k and ϵ is given by

$$\mu_t = \rho\, C_\mu \frac{k^2}{\epsilon}, \tag{20}$$

where C_μ is a value that varies according to the used $k - \epsilon$ model.

Furthermore, a quantity S appears in the $k - \epsilon$ models. This quantity is defined by

$$S = \sqrt{2 S_{ij} S_{ij}}, \tag{21}$$

where S_{ij} is the strain rate tensor:

$$S_{ij} = \frac{1}{2}\left(\frac{\partial \bar{u}_i}{\partial x_j} + \frac{\partial \bar{u}_j}{\partial x_i}\right). \tag{22}$$

The two $k - \epsilon$ models employed in the present work are detailed below.

2.2.1 Standard $k - \epsilon$ model

The standard $k - \epsilon$ model was proposed by Launder and Spalding (1972). It is a semi-empirical model quite popular in simulating industrial problems due to its robustness, economy and reasonable accuracy. As previously commented, the standard $k - \epsilon$ model is a two-equation model based on the transport of the turbulence kinetic energy and its dissipation rate, which derivation depends on physical and empirical considerations.

The turbulent kinetic energy can be calculated by Eq. (18) where the production term P_k and the dissipation term D_k are

$$P_k = \mu_t S^2, \tag{23a}$$

$$D_k = -\rho\epsilon. \tag{23b}$$

However, the dissipation rate is given in Eq. (19) with the production term P_ϵ and the dissipation term D_ϵ equal to

$$P_\epsilon = C_{\epsilon 1}\frac{\epsilon}{k}\mu_t S^2, \tag{24a}$$

$$D_\epsilon = -\rho C_{\epsilon 2}\frac{\epsilon^2}{k}. \tag{24b}$$

The model coefficients are $\sigma_k = 1.0,\ \sigma_\epsilon = 1.3,\ C_\mu = 0.09$, $C_{\epsilon 1} = 1.44$ and $C_{\epsilon 2} = 1.92$.

2.2.2 Realizable $k-\epsilon$ model

Shih *et al.* (1993) proposed a new formulation for the turbulent viscosity and for the transport equation of ϵ. The model was called realizable $k-\epsilon$ and it presents greater mathematical consistency on the Reynolds stress tensor than the standard $k-\epsilon$ model, in certain restrictions.

In this model, the production and dissipation terms for the transport equations of k and ϵ are

$$P_k = -\rho\overline{u_i u_j}\frac{\partial \bar{u}_i}{\partial x_j}, \tag{25a}$$

$$D_k = -\rho\epsilon, \tag{25b}$$

$$P_\epsilon = -\rho\, C_{\epsilon 1}\,\frac{k}{\epsilon}\,\overline{u_i u_j}\,\frac{\partial \bar{u}_i}{\partial x_j}, \tag{26a}$$

$$D_\epsilon = -\rho\, C_{\epsilon 2}\frac{\epsilon^2}{k}, \tag{26b}$$

in which $\overline{u_i u_j}$ are the Reynolds stresses given by

$$\overline{u_i u_j} = \frac{2}{3}k\delta_{ij} - C_\mu\frac{k^2}{\epsilon}2S^*_{ij} + 2C_2\frac{k^3}{\epsilon^2}(-S^*_{ik}\Omega_{kj} + \Omega_{ik}S^*_{kj}), \tag{27}$$

where

$$S^*_{ij} = S_{ij} - \frac{1}{3}S_{kk}\delta_{ij}, \tag{28}$$

and

$$\Omega_{ij} = \frac{1}{2}\left(\frac{\partial \bar{u}_i}{\partial x_j} - \frac{\partial \bar{u}_j}{\partial x_i}\right). \tag{29}$$

The model constants are $C_{\epsilon 1} = 1.44,\ C_{\epsilon 2} = 1.92,\ \sigma_k = 1.0$ and $\sigma_\epsilon = 1.2$. The C_μ term is considered as a constant in the standard $k-\epsilon$ model. However, this term is calculated for each time step, in the realizable $k-\epsilon$ model, using the following formulation

$$C_\mu = \frac{1}{A_0 + A_s U^* \frac{k}{\epsilon}}, \tag{30}$$

where

$$U^* = \sqrt{S_{ij}S_{ij} + \Omega_{ij}\Omega_{ij}}, \tag{31}$$

$A_0 = 4.04$ and

$$A_s = \sqrt{6}\,cos\phi, \tag{32}$$

in which

$$\phi = \frac{1}{3}arccos(\sqrt{6}\,W), \tag{33a}$$

$$W = \frac{S_{ij}S_{jk}S_{ki}}{\tilde{S}^3}, \tag{33b}$$

and

$$\tilde{S} = \sqrt{S_{ij}S_{ij}}. \tag{33c}$$

In Eq. (27), there is another coefficient C_2 calculated dynamically in each time step based on flow properties, which is given by

$$C_2 = \frac{\sqrt{1 - 9\,C_\mu^2\left(\frac{S^*k}{\epsilon}\right)^2}}{C_0 + 6\,\frac{S^*k}{\epsilon}\frac{\Omega^*k}{\epsilon}}, \tag{34}$$

where $C_0 = 1.0$,

$$S^* = \sqrt{S^*_{ij}S^*_{ij}}, \tag{35a}$$

and

$$\Omega^* = \sqrt{\Omega_{ij}\Omega_{ij}}. \tag{35b}$$

According to Shih *et al.* (1993), the realizable $k-\epsilon$ model can predict the spreading rate of plane and round jets well.

3. COMPUTATIONAL SIMULATIONS

For the present work, the MFSim code is employed. The MFSim is an "in-house" code developed in the Laboratory of Fluid Mechanics (MFLab) from the Federal University of Uberlandia (UFU). The base of the MFSim is an adaptive block-structured regular and cartesian mesh which reduces the computational cost. To treat the turbulence, in this code the Large Eddy Simulation (LES) models and Unsteady Reynolds Average Navier-Stokes (URANS) models are available to the user. It is possible to simulate problems like fluid-structure interaction, multiphase flows, reactive and turbulent flows considering 3D domains and parallel processing using MFSim (Neto *et al.*, 2019; Melo *et al.*, 2018; Gasche *et al.*, 2012; Denner *et al.*, 2014).

In the MFSim code, the Navier-Stokes equations are solved for incompressible flows, Eqs. (2) and (3). These equations are discretized using the finite volume method in a staggered grid. The Semi Backward Difference Formula (SBDF) method is used in the temporal discretization of the transport equations (Wang and Ruuth, 2008). This method is based on a semi-implicit discretization, in which the advective term is treated explicitly and the difusive term is treated implicitly. For the advective term, the Convergent and Universally Bounded Interpolation Scheme for the Treatment of Advection (CUBISTA) is applied (Alves *et al.*, 2003). Besides that, for the diffusive term, the Central Differencing Scheme (CDS) is used (Fergizer and Peric, 2002).

The computational domain was defined according to the schematic representation shown in Fig. 1. The whole domain was solved using a grid with one refinement level and 6 cells per diameter.

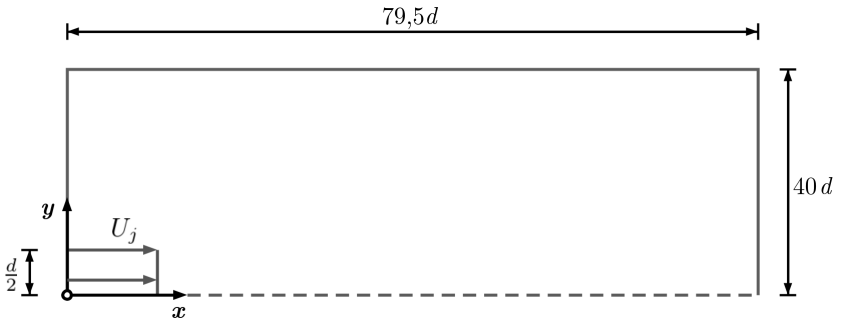

Figure 1: Computational domain used in the jet simulations.

The inlet fluid flow enters the domain with a mean velocity of $U_j = 56.2$ m/s. A turbulence intensity of $0.58\,\%$ was assumed based on Hussein *et al.* (1994). The physical properties of the fluid were set as $\rho = 1$ kg/m^3 and $\mu = 4.443{\times}10^{-5}$ Pa·s to match a Reynolds number of 9.55×10^4. The CFL was set to 0.2. Lastly, the boundary conditions were imposed as shown in Tab. 1. It should be emphasized that the applied Neumann conditions were homogeneous.

Table 1: Boundary conditions applied in the domain.

Domain faces	u	v	w	p	k	ϵ
West	Dirichlet	Dirichlet	Dirichlet	Neumann	Dirichlet	Dirichlet
East	Neumann	Neumann	Neumann	Dirichlet	Neumann	Neumann
South	Neumann	Neumann	Neumann	Dirichlet	Neumann	Neumann
North	Neumann	Neumann	Neumann	Dirichlet	Neumann	Neumann
Bottom	Periodic	Periodic	Periodic	Periodic	Periodic	Periodic
Top	Periodic	Periodic	Periodic	Periodic	Periodic	Periodic

4. RESULTS

Figure 3 shows the velocity decay profiles at the jet centerline obtained with the computational simulations and the continuous solution, that were compared with the experimental results of Van der Hegge Zijnen (1958). Figure 2 shows the comparison of the velocity profile along y direction, $\bar{u}(x, y)$ at different distances of the nozzle between computational simulations, continuous solution and experimental data provided by Heskestad (1965) and Bradbury (1965).

In order to analyze the continuous solutions, the profiles given by Eqs. (17) and (15) were compared with experimental data obtained by different authors. The continuous solution for jet center line decay was compared with Van der Hegge Zijnen (1958) experimental data and it presented values of 0.024 and 0.012 for the L_∞ and L_2 norms, respectively. The dimensionless velocity profile, given by Eq. (15), presented $L_2 = 0.043$ and $L_\infty = 0.072$, when compared with Bradbury (1965) experimental data for $x = 60\,d$ (Fig. 2b).

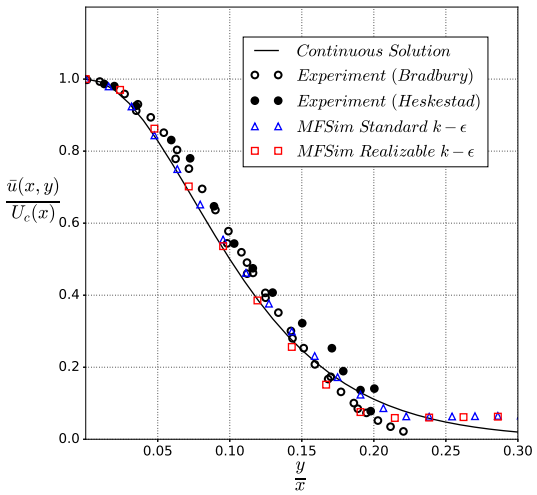

(a) $x = 50\,d$

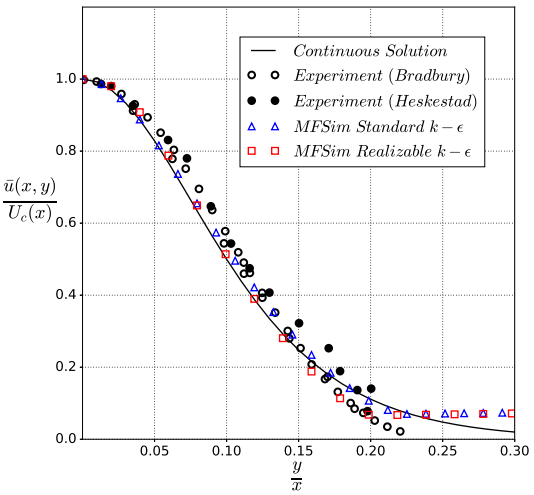

(b) $x = 60\,d$

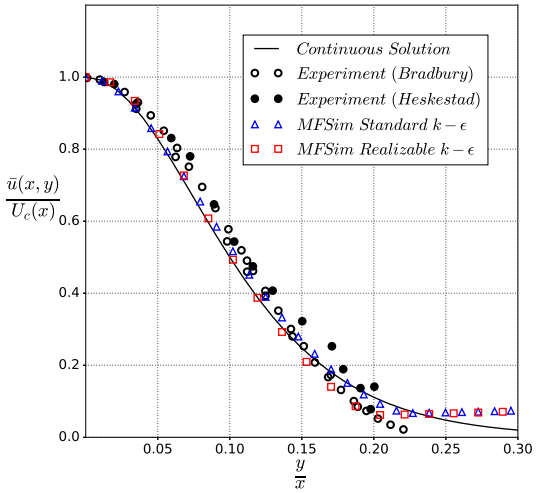

(c) $x = 70\,d$

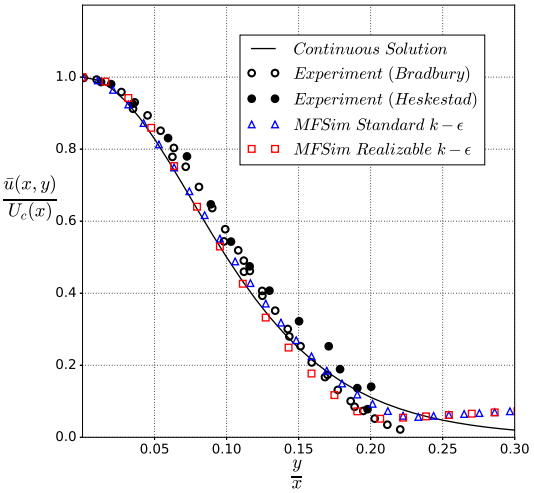

(d) $x = 75\,d$

Figure 2: Comparison of $\bar{u}(x, y)$ profile considering different distances from the jet nozzle.

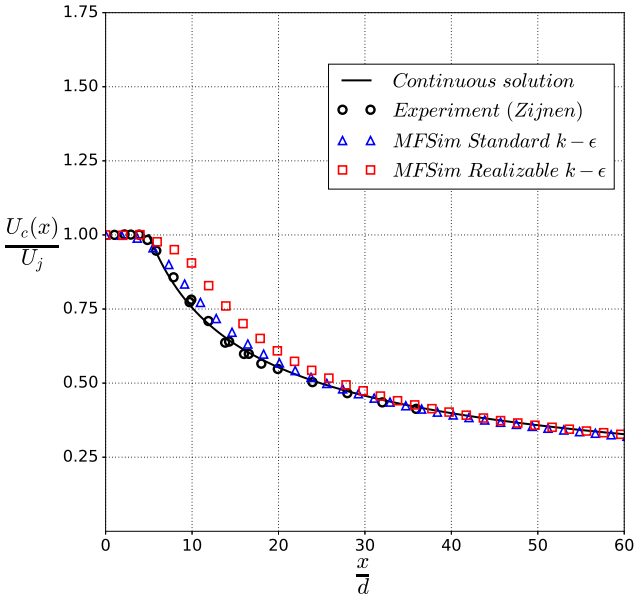

Figure 3: Comparison of jet centerline velocity profile.

5. CONCLUSIONS

About the continuous solutions, the profiles presented a good agreement with experimental data for the jet velocity profile, $\bar{u}(x, y)$, and jet centerline velocity, $U_c(x)$. The continuous solutions can be a good tool for the validation process in computational codes.

As discussed previously, simulations were performed using two variations of $k - \epsilon$ models in order to compare the results with the profiles obtained through the continuous solutions and experimental data. Analyzing the results shown in Fig. 3 and Fig. 2 ,it was observed that the standard $k - \epsilon$ model presented better performance to predict the velocity decay of the jet center line. In order to predict the radial velocity profile and the spreading rate, the realizable $k - \epsilon$ was more in agreement with the continuous solution, while the standard model presented better agreement with the experimental data as shown in Fig. 2.

Finally, it can be concluded that no model is better than the other in a general way. However, it is important to choose the model according to the characteristics and properties of the flow based on the desired accuracy.

6. ACKNOWLEDGEMENTS

The authors acknowledge CAPES, Petrobras, CNPq and FAPEMIG for their support of this work.

7. REFERENCES

Alves, M., Oliveira, P. and Pinho, F., 2003. "A convergent and universally bounded interpolation scheme for the treatment of advection". *International Journal for Numerical Methods in Fluids*, pp. 47–75. doi:10.1002/fld.428.

American Society of Heating, R. and Engineers, A.C., 1989. *1989 ASHRAE Handbook: Fundamentals*. Ashrae handbook series. ASHRAE. ISBN 9780910110563. URL `https://books.google.com.br/books?id=_oWwDQEACAAJ`.

Andrade, E.d.C., 1939. "The velocity distribution in a liquid-into-liquid jet. part 2: The plane jet". *Proceedings of the Physical Society*, Vol. 51, pp. 784–793.

Block, N.R., 2006. *Comparison of Mixing Length, Standard k-epsilon, and Renormalized Group k-epsilon Turbulence Models in GOTHIC 7.2*. Ph.D. thesis, North Carolina State University.

Bradbury, L., 1965. "The structure of a self-preserving turbulent plane jet". *Journal of Fluid Mechanics*, Vol. 23, No. 1, pp. 31–64.

Denner, F., van der Heul, D.R., Oud, G.T., Villar, M.M., da Silveira Neto, A. and van Wachem, B.G., 2014. "Comparative study of mass-conserving interface capturing frameworks for two-phase flows with surface tension". *International Journal of Multiphase Flow*, Vol. 61, pp. 37–47.

Fergizer, J.H. and Peric, M., 2002. *Computational Methods for Fluid Dynamics*. Springer.

Gasche, J.L., Barbi, F. and Villar, M.M., 2012. "An efficient immersed boundary method for solving the unsteady flow through actual geometries of reed valves".

Heskestad, G., 1965. "Hot-wire measurements in a plane turbulent jet". *J. Appl. Mech*, Vol. 32, No. 4, p. 721.

Hussein, H.J., Capp, S.P. and George, W.K., 1994. "Velocity measurements in a high-reynolds number, momentum-conserving, axisymmetric, turbulent jet". *Journal of Fluid Mechanics*, pp. 31–75.

Lam, C. and Bremhorst, K., 1981. "A modified form of the k-ε model for predicting wall turbulence". *Journal of fluids engineering*, Vol. 103, No. 3, pp. 456–460.

Launder, B.E. and Spalding, D.B., 1972. *Lectures in Mathematical Models of Turbulence*. Academic Press.

Liu, Q., Hoff, S.J., Maxwell, G.M. and Bundy, D.S., 1996. "Comparison of three ke turbulence models for predicting ventilation air jets". *Transactions of the ASAE*, Vol. 39, No. 2, pp. 689–698.

Melo, R., Kinoshita, D., Villar, M., Serfaty, R. and Silveira-Neto, A., 2018. "Simulation of thermal transfer using the immersed boundary method and adaptive mesh". In *ICHMT DIGITAL LIBRARY ONLINE*. Begel House Inc.

Neto, H.R., Cavalini, A., Vedovoto, J., Neto, A.S. and Rade, D., 2019. "Influence of seabed proximity on the vibration responses of a pipeline accounting for fluid-structure interaction". *Mechanical Systems and Signal Processing*, Vol. 114, pp. 224–238.

Shih, T.H., Zhu, J. and Lumley, J.L., 1993. "A realizable reynolds stress algebraic equation model". *Ninth Symposium on Turbulence Shear Flows Kyoto*.

Ströher, G.R., Lima, R.C., de Andrade, C.R. and Zaparoli, E.L., 2009. "Evaluation of the capability of the rans turbulence model to account for the effects of the variations of the nozzle condition for a round free jet flow".

Tennekes, H. and Lumley, J.L., 1972. *A first course in turbulence*. MIT press.

Van der Hegge Zijnen, B., 1958. "Measurements of the velocity distribution in a plane turbulent jet of air". *Applied Scientific Research*, Vol. 7, No. 4, pp. 256–276.

Wang, D. and Ruuth, S., 2008. "Variable step-size implicit-explicit linear multistep methods for time-dependent partial differential equations". *Journal of Computational Mathematics*, pp. 838–855. URL `http://hdl.handle.net/2142/18708`.

Wilcox, D.C., 1994. *Turbulence modeling for CFD*. DCW Industries Inc.

8. RESPONSIBILITY NOTICE

The authors are the only responsible for the printed material included in this paper.